



Ignition and combustion analysis of direct write fabricated aluminum/metal oxide/PVDF films



Miles C. Rehwoldt^{a,b}, Haiyang Wang^b, Dylan J. Kline^{a,b}, Tao Wu^a, Noah Eckman^a, Peng Wang^a, Niti R. Agrawal^a, Michael R. Zachariah^{b,*}

^a University of Maryland, College Park, MD, USA

^b University of California, Riverside, CA, USA

ARTICLE INFO

Article history:

Received 3 May 2019

Revised 13 August 2019

Accepted 14 August 2019

Keywords:

Films

Energetics

3D printing

Nanoparticles

ABSTRACT

Metallized energetic composite films incorporating high mass loadings of aluminum nanoparticle fuels and metal oxide oxidizers (thermite) within a polyvinylidene fluoride (PVDF) polymer matrix were constructed via repeatable direct write additive manufacturing (3-D Printing). High speed videography, Temperature-Jump/Time of Flight Mass Spectrometry (T-Jump/TOFMS), and 2D spatiotemporal temperature mapping were used to analyze the role of composition and particle loading with respect to ignition behavior and combustion performance. This study reveals that, while the ignition temperatures of films are relatively unvaried in pressurized environments, ignition temperatures in vacuum are strongly dependent on the inclusion of thermite material and the specific type of thermite utilized. Increasing thermite mass loading results in a reduction in film flame speed and mechanical integrity but increases flame temperature. Coupled time of flight mass spectrometry reinforces and elaborates on previous findings regarding the Al/PVDF reaction mechanism as it pertains to the coupled behavior of incorporating increasing amounts of metal oxides. TOFMS highlights carbon dioxide generation from the metal oxide interaction with PVDF, leading to unintended stoichiometric considerations and distinct changes in steady burn behavior which contribute adverse factors towards flame propagation.

© 2019 Published by Elsevier Inc. on behalf of The Combustion Institute.

1. Introduction

The fabrication of solid propellants employing metallic nanoparticles as an energy dense fuel has become a promising frontier in the search for novel materials with the potential for enhanced energy release rates. In recent years, the draw to research metal nanoscale energetics stems from their theoretically greater chemical energy density compared to traditional CHNO chemistry [1]. Despite reaction enthalpy considerations, reaction kinetics of traditional micron scale solid energetics are relatively slow, limited by the diffusion length scales between fuel and oxidizer. Contemporary formulations utilizing nanoscale fuels and oxidizers seek to increase specific surface area and reduce characteristic diffusion length scales for enhanced reactivity to approach that of molecular monopropellants such as 2,4,6-trinitrotoluene (TNT).

Studies utilizing metal particles for energetic purposes commonly use aluminum nanoparticles as the fuel for metallized energetic composites due to its light weight, superior combustion

enthalpy, and cost effectiveness compared to alternative nanoscale metal fuels such as titanium and tantalum. Formulations for solid propellants typically involve high mass loadings of reactive material incorporated into a polymer binder such as polyvinylidene fluoride (PVDF), nitrocellulose (NC), and hydroxyl-terminated polybutadiene (HTPB) [2–5]. Recently, fluorine containing polymer binders, such as PVDF and THV (copolymer of tetrafluoroethylene, hexafluoropropylene and vinylidene fluoride), have come to the forefront of experimentation and application due to their ability to act as a reactive binder in the formation of Al-F bonds [6–8]. The fluoropolymer PVDF is primarily utilized for its mechanical strength, thermal stability, and solubility in a suitable solvent for expanded materials processing [8]. From previous studies, it was shown that early onset fluoropolymer decomposition occurs through a gas phase exothermic pre-ignition reaction with the aluminum oxide shell, exposing the aluminum core to further fluorination [8–10].

Thermite systems (metal/metal oxide) have also been the focus of several studies as a means for high energy release for a variety of applications for which reactivity and flame speeds are enhanced when utilizing nanomaterials [2,6,11,12]. The metal oxides (MO) considered in this study are copper(II) oxide,

* Corresponding author.

E-mail address: mrz@engr.ucr.edu (M.R. Zachariah).

bismuth(III) oxide, and iron(III) oxide. While Fe_2O_3 is the most common oxidizer for traditional thermite systems, CuO is a well-studied gas phase oxidizer with favorable heat of formation, and Bi_2O_3 is a known condensed phase oxidizer with high oxygen ion mobility [13–15]. This study assesses the ability to tune the energy release of stoichiometric aluminum–fluoropolymer propellant systems by incorporating nano-scale thermites at various mass loadings. Analysis of both intended and unintended consequences with respect to the fabrication process, chemistry, composite morphology, and apparent mechanical properties were documented.

In the past decade, additive manufacturing (AM) has been an increasingly active field of research in several disciplines with applications and research within the energetics community becoming more viable and sought out [16]. The draw to additive manufacturing manifests from the desire for flexibility, potential scale up, and the ability to reproduce unique and highly customizable architectures in the most cost effective and efficient manner [16]. Although additive manufacturing of aluminum containing polymers has been recently explored by other studies [4,5,17–20], we employed a solvent-based extrusion, layer-by-layer additive manufacturing technique to fabricate thermite integrated energetic materials from a precursor solution. This method utilizes a suitable solvent to dissolve the polymer binder and allow for thorough mixing with suspended particles. We apply this additive manufacturing technique for polymer printing, explicitly described in the study conducted by Manjot et al., to allow for wide precursor variations with respect to viscosity, employed solvent, and solid loading [21]. The controlled translation and extrusion dynamics inherent to 3D printing allows for increased degrees of freedom for energetic materials to be printed quickly and precisely into a variety of patterns, shapes, and (micro)structures which may be characterized by Scanning Electron Microscopy (SEM).

The combination of high-speed videography, thermometry, and time of flight mass spectrometry diagnostics were utilized to probe and analyze important ignition characteristics and potential throttling behavior of energetic propellants integrated with readily available and well-studied nanoscale metal oxides. The results of this study may be used for future studies which focus on tunable architectures provided by this method of AM to probe the structure–function relation of film combustion performance complementary to the behavior of reactive film constituents.

2. Methods/Experimental

2.1. Materials

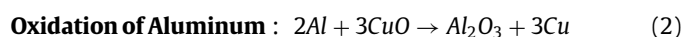
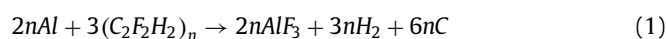
Aluminum nanoparticles (nAl) (~80 nm) used in this study were purchased from Novacentrix. It was determined from thermogravimetric analysis (TGA) that the passivated aluminum nanoparticles are 81% active by mass. Nanoparticle metal oxide oxidizers in the form of CuO (<50 nm), Fe_2O_3 (<50 nm), and Bi_2O_3 (90–210 nm) were purchased from Sigma Aldrich (Millipore Sigma). Poly(vinylidene fluoride) powder (PVDF) (MW = 534,000) was also purchased from Sigma Aldrich (Millipore Sigma) and N,

N-dimethylformamide (DMF 99.8%) solvent was purchased from BDH chemicals. All chemicals were used as received.

2.2. Film fabrication

Energetic composites were fabricated using a System 30 M pressure driven 3D printer purchased from Hyrel 3D. The low viscosity (~0.1 Pa·s) energetic precursor was utilized as a 3D printable ink in a direct write approach. Each precursor ink considered was formulated by dissolving a constant 100 mg/ml PVDF in DMF and adding the appropriate stoichiometric mass content of metal fuel and oxidizer Eqs. (1–4). The concentration of PVDF in DMF and level of particles suspended was chosen based off of previous studies in our group using electrospray for fabrication of similar films [3,7].

Binder Fluorination of Aluminum :



Stoichiometric mixtures of aluminum oxidized by metal oxide components incorporated within the films were considered by treating the parallel Al/PVDF reaction and thermite reaction as being mutually exclusive Eqs. (1–4). The individual mixtures and particle loadings are listed in Table 1 where the specific loadings correlate to 1/4 wt. content (no added thermite), 1/2 wt. content (low thermite loading), and 2/3 wt. content (high thermite loading) of total nanoparticle material in the films. These weight percentages were chosen to better observe the effects that the metal oxides may introduce as well as to test the previously documented mass loading limits of PVDF bound nanopowders [3]. Precursor suspensions are sonicated up to 2 h for each component added, depending on particle loading, then left to stir for 24 h using a magnetic stir plate/bar. Before printing, precursor inks are sonicated for 1 h then loaded into a 30cc disposable syringe equipped with a 21-gauge blunt Luer Lock needle and mounted to the extrusion pump of the 3D printer. Before printing, the ink is primed, and the glass printing bed heated to as high as 85 °C. Since the ink is in liquid form, the programmed printing routine is optimized for solvent evaporation before subsequent layer deposition. The drying process can be controlled by the temperature of the printing bed, the speed and extrusion rate of the print, and/or the volatility of the chosen solvent. Dry times for our prints were on the order of 10–15 s per pass. In order to study the 1D combustion performance of our materials, we printed single line strands with a width roughly equivalent to the outer diameter of the extrusion needle (0.8 mm). Individual layer thickness may range between 5–20 μm/layer and depends strongly on the print speed and specific flow parameters (0.5–5 ml/hr). Multiple 3 cm long strands, like those in Figure S1c,

Table 1
Energetic precursor formulations.

| Al Fuel (wt.%) | PVDF (wt.%) | Added Oxidizer: (wt.%) | Total Particle Loading (wt.%) |
|----------------|-------------|--------------------------------|-------------------------------|
| 25 | 75 | -- | 25 |
| 20.8 | 50 | Bi_2O_3 : 29.2 | 50 |
| 23.9 | 50 | CuO : 26.1 | 50 |
| 26.5 | 50 | Fe_2O_3 : 23.5 | 50 |
| 18.1 | 33.3 | Bi_2O_3 : 48.6 | 66.7 |
| 23.2 | 33.3 | CuO : 43.5 | 66.7 |
| 27.5 | 33.3 | Fe_2O_3 : 39.2 | 66.7 |

were harvested from a larger 25 cm perimeter rectangular structure printed and carefully peeled from the glass printing bed. Film porosity estimations were made using Eqs. (5) and (6) given their composition mass fractions (χ_i) as well as their theoretical and measured densities (ρ_{th} & ρ_m) for which these estimates are displayed in Table S1 [3].

$$P = 1 - \frac{\rho_m}{\rho_{th}} \quad (5)$$

$$\rho_{th} = \sum_i \chi_i \rho_i \quad (6)$$

2.3. Characterization

Films in this study were characterized based on their physical properties and reaction properties. Physical properties considered included thickness, reproducibility, morphology, mechanical integrity, and composition. Reaction properties considered included self-propagating combustion performance in an anaerobic environment, ignition in pressured and vacuum conditions, and the content of their condensed phase combustion products.

Cross-sections and top surfaces of each film are analyzed using Scanning Electronic Microscopy (SEM, Hitachi, SU-70 FEG-SEM) and compared to one another. Properties of precursor inks were characterized using an AR2000 rheometer mounted with a 40 mm 2" steel cone and the tensile strength of single layer films measured using a Shimadzu Autograph AGS-X tensile tester.

For each film formulation, combustion was conducted in argon (~1 atm) and repeated in triplicate. A small cylindrical chamber with a gas valve inlet and outlet was purged with argon for 5–10 min and a mounting rod used to hold the films in place (Figure S2). Film geometry was strictly maintained with approximately the same thickness, $(70 \pm 3) \mu\text{m}$, width, 0.8–1 mm, and length, 3 cm. Each film strand is sandwiched between two braided nichrome wires and anchored at the opposite end with double-sided tape. Films are ignited within the argon chamber using the nichrome wire and the combustion performance assessed using a Phantom v12.0 high-speed digital camera operating at 3000 (zoomed out view) and 10,000 (zoomed in view) frames per second (FPS) with an exposure of 200 and 20 μs , respectively. Self-propagating characteristic flame speeds are measured using videos processed in ImageJ manual tracking to obtain time resolved positions using data points with a known pixel to distance ratio at every 25–50 frames (Figure S3c). Two out of place gaps in the example data in Figure S3c represent the precisely spaced metal gratings in the foreground which block light from the flame at certain positions.

Temperature dependent reaction chemistry and possible mechanisms were diagnosed by conducting T-Jump/Time of Flight Mass Spectrometry (T-Jump/TOFMS) and implementing the diagnostic technique of Color Camera Pyrometry (CCP) described in our groups previous work [22]. CCP offers a post-processing method by which the grey body emissions of the film flame-front, as captured by the Bayer filter of the color camera, are processed to return 2-D temperature maps of the flame front as a function of time [22]. T-Jump/TOFMS offers a method by which transient gas phase species can be detected prior to and after the potential ignition event on the timescale of a combustion event. The technique of T-Jump/TOFMS is outlined explicitly in previously published papers from our group in which a sufficiently thin layer of material ($<3 \mu\text{m}$) is printed directly onto a thin platinum wire (76 μm), illustrated in Figure S4, and rapidly heated ($\sim 3 \times 10^5 \text{ K/s}$) in a vacuum chamber (10^{-6} Torr) to temperatures as high as 1400 K [8,23]. Rapid heating is temporally coupled to species detecting mass spectrometry (100 μs /spectrum) and ignition visualizing high speed videography (10^5 FPS -10 μs exposure) [24]. Solid phase species of combustion products are collected

for X-ray diffraction (XRD, Bruker C2 Discover, CuK α sealed X-ray tube) and SEM/EDS analysis to confirm possible reaction mechanisms for self-propagation.

3. Results and discussion

3.1. Fabrication Al/MO/PVDF films

Al/PVDF films are highly reproducible in both thickness and uniformity with respect to morphology through the direct write approach. SEM/EDS images in Fig. 1a show that film cross-sections have a high degree of homogeneity between aluminum and PVDF. SEM cross-section analysis of 5-layer films containing thermite materials incorporating 50 wt.% particle loading are shown in Fig. 1b–d. Despite the difference of metal oxide type and relative particle size range, each formulation printed with 5 layers resulted in films with predictable XRD patterns, nearly identical thickness, roughly 70 μm ($\sim 14 \mu\text{m}/\text{layer}$), and consistent uniformity. The same cannot be said, however, for 67 wt.% particle loading films for which their morphology will be discussed in a later section of this paper.

The second row of each column of Fig. 1b–d reveals the contrast between the aluminum and metal oxide nanoparticles from SEM electron backscattering of heavier elements. Comparisons of the Bi_2O_3 and CuO particle sizes in relation to aluminum particles in Fig. 1 show that although CuO nanoparticles are quoted to be smaller than 50 nm by Sigma Aldrich, they appear to have roughly the same distinct aggregate size as Bi_2O_3 particles (90–210 nm). Transmission Electron Microscopy (TEM) images of as received metal oxide particles in Figure S5 shows that CuO nanoparticles have smaller primary structures than Bi_2O_3 , but are irregularly shaped with a higher degree of aggregation behavior compared to Fe_2O_3 nanoparticles. This leads to the conclusion that CuO particles lack of particle dispersion, either physically or chemically, leads to hindered dispersion of CuO particles in Al/PVDF films. Fe_2O_3 nanoparticles shown in Fig. 1, unlike CuO and Bi_2O_3 particles, appear to be indistinguishable from aluminum in both color contrast and particle size. From Figure S5 and Figure S6, Fe_2O_3 particles at 50 wt.% particle loading appear to have superior dispersion behavior of much smaller particles with no obvious regions of severe agglomeration.

Higher mass loadings of thermite material (67 wt.%) were added to the stoichiometric Al/PVDF mixture to study whether film performance can be enhanced with an increase in thermite density. Generally, adding more nano-scale particles has adverse effects during the printing process [25]. The effects that each particle type has on printability and resulting film morphology becomes more apparent at higher mass loading [5].

The effects of printing film precursors with increasing amounts of nanomaterials include the following:

- Increased ink viscosity leading to increased likelihood that the printer nozzle will be clogged if the flowrate is below a certain threshold [5].
- Shear rate-controlled viscosity measurements of select precursor inks extruded at pipe flow shear rates on the order of 10^{-1} – 10^2 s^{-1} show viscosities between 0.1–10 Pa·s while printing (Figure S7).
- Ink with the highest nanoparticle loading and smallest primary particle size displays viscosity values four orders of magnitude higher than the viscosity of the low particle loading ink, but with clear shear thinning behavior (Figure S7).

Added nano-materials to precursor formulations results in the following observations to the characteristics of the product films:

- Other than the increased film density of the metal oxide species, composites with higher mass loading convey no

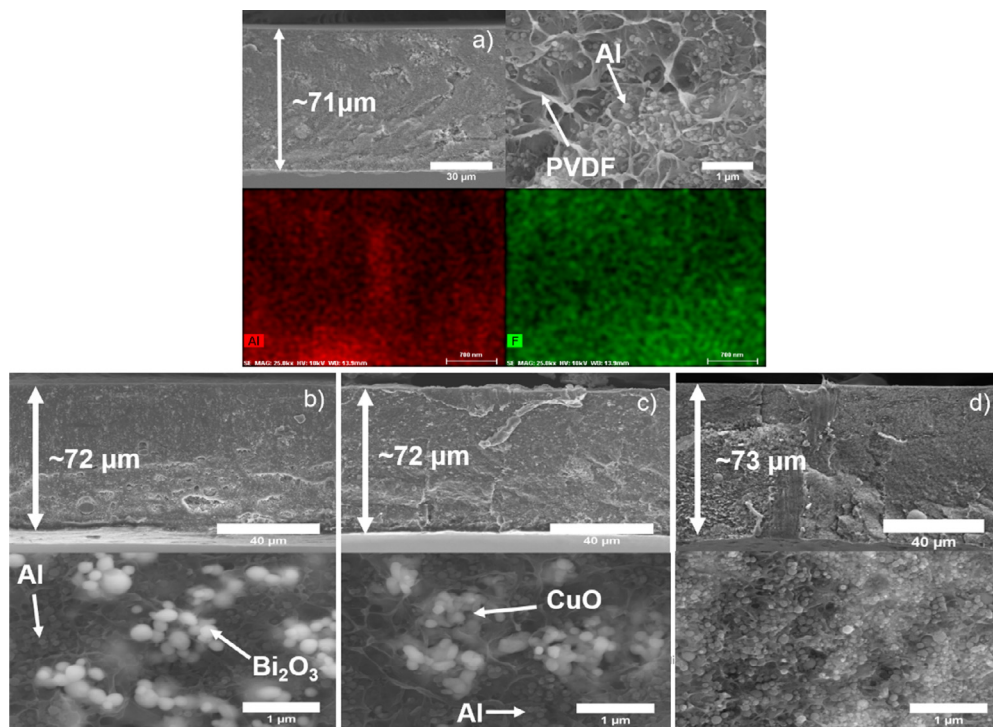


Fig. 1. SEM cross-section of 5-layer ($\sim 14\mu\text{m}/\text{layer}$) 3D printed a) Al/PVDF, b) Al/Bi₂O₃/PVDF, c) Al/CuO/PVDF, and d) Al/Fe₂O₃/PVDF Films.

significant difference in constituent homogeneity compared to the lower mass loading (Figure S6).

- Reduction in mechanical integrity and increase in film porosity formed due to rapid solvent evaporation, leading to extremely brittle films with irregular thickness profiles (Figure S8–S10) (Table S1).
- Small particle size, number of particles, and particle dispersiveness allows for enhanced intimacy with the polymer binder, causing a degradation in polymer elasticity and its ability to relax after vaporized solvent has displaced material (Figure S8–S10).
- Considering the density of the metal oxide type (Bi₂O₃ > CuO > Fe₂O₃) and particle size (Bi₂O₃ > CuO \geq Fe₂O₃) (Figure S5), this order also reflects the gradual reduction in mechanical integrity (Bi₂O₃ > CuO > Fe₂O₃) (Figure S9–S10).

3.2. Film combustion

3D printed films often have similar physical appearances, but their combustion performance and behavior are quite different. A zoom in of propagation snapshots captured at 10,000 FPS are displayed in Fig. 2a and the flame speed results of all compositions studied shown in Fig. 2b and c. Due to its severe geometric inconsistencies shown in Figure S10c, the highest film loading of Fe₂O₃ was not considered for these measurements.

All combustion events are steady burning with a curved flame front. As Figure S11 illustrates, the characteristic combustion behavior of each composition can vary in terms of how product material is shed as thermite mass loading changes. The Al/PVDF composite appears to retain its burned material for a much longer time, curling on top of itself at times shown in Figure S11a. As thermite content increases, material just behind the flame front is torn away and ejected at greater speeds (1–10 m/s), outlining a much clearer and thinner flame front (Figure S11e–S11f). Another interesting feature at the high loading of thermite content was the repeated observance of the flame to burn in a manner which fa-

vored one side of the film with a slanted flame front shown in Figure S11e. Although this behavior persisted for reasons unknown to us, flame fronts were still steady burning with flame morphology maintained and simply translating in time linearly. Further analysis of this behavior by Time of Flight Mass Spectrometry and Colored Camera Pyrometry will show that these observations are likely due to the sudden generation of nascent gaseous species originating in some capacity from the added metal oxides [26], carrying away still burning material which would otherwise contribute to the forward propagation of energy. This behavior would thus be intensified as more thermite content is incorporated and films become increasingly porous.

Figure 2c illustrates the hierarchy of combustion performance which is independent of the metal oxide species utilized. Homogeneously incorporating thermite material within Al/PVDF films does not lead to enhanced burn speeds. As Fig. 3 shows, XRD and EDS characterization of films burned in argon finds no evidence for any remaining reactant species with respect to aluminum and the corresponding metal oxide. These finds were the same for both thermite loadings.

Evidence from EDS line scan characterization in Fig. 3 shows that aluminum interacts with both the metal oxide and PVDF. The cubic AlF₃ and coalesced Al₂O₃-reduced metal product structures exist within the immediate vicinity of one another [3,17]. Along with potential changes to composite dependent thermal diffusivity, it is likely that the kinetics of the Al/PVDF reaction are faster than the Al/MO reaction due to PVDF proximity and the relatively low temperature of the Al-PVDF pre-ignition reaction [8]. As a result, aluminum directly adjacent to PVDF would be consumed readily, increasing the characteristic length scale for which oxygen from the metal oxide would need to traverse to react with the remaining aluminum. The Al/PVDF reaction would thus be the main reaction driving flame propagation with the Al/MO reaction occurring just behind the flame front. The proposed burning mechanism based on observations already conveyed in this paper, and those discussed later, is illustrated in Fig. 4.

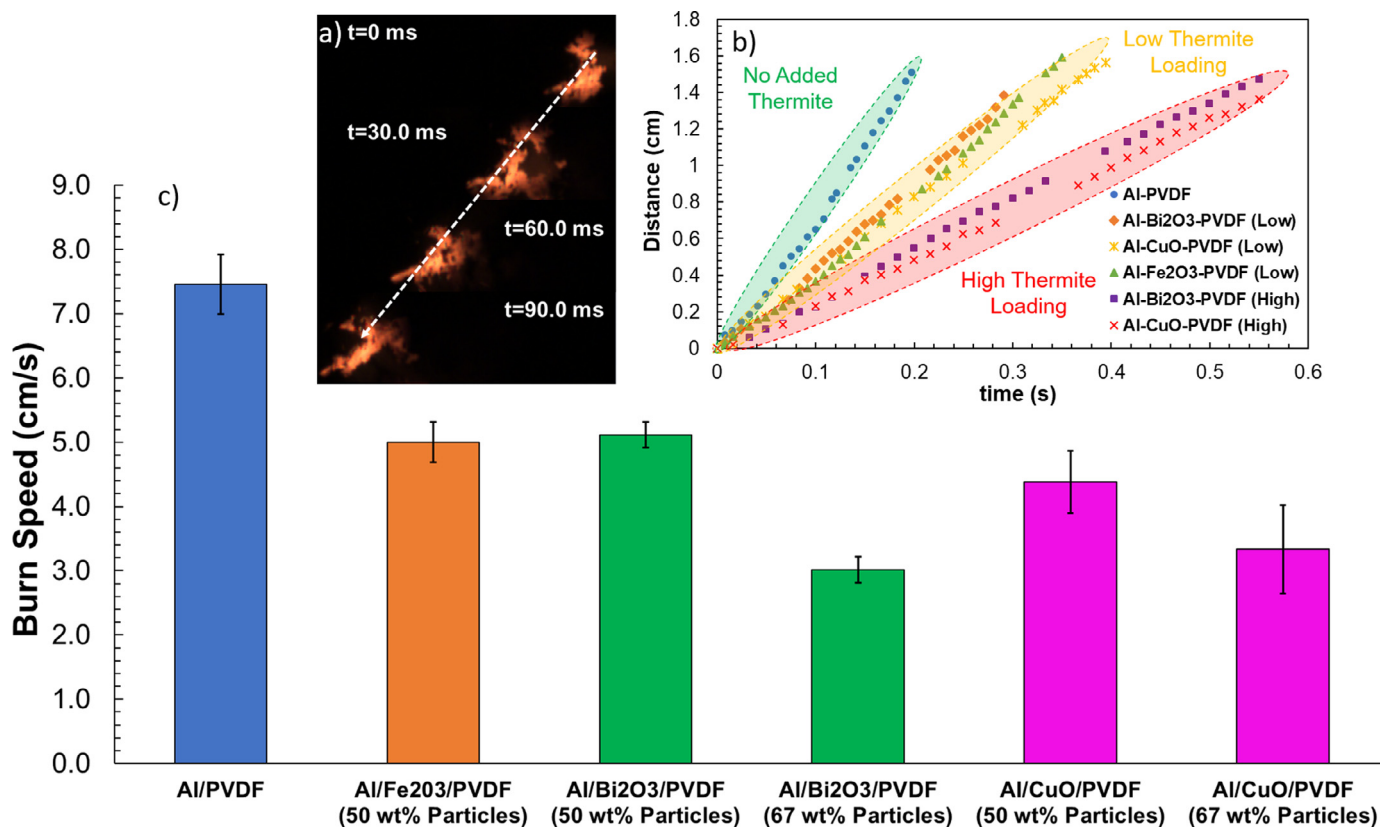


Fig. 2. a) Snap shots of steady flame propagation of Al/CuO/PVDF with 50 wt.% particle loading accompanied by b) representative linear distance over time plots of each composition. Averaged flame speed results are consolidated in a c) comparative bar graph.

Color Camera Pyrometry (CCP) post-processing of the high-speed videos was applied to gain more insight into the flame temperature and energy release of each corresponding film composition. Through CCP we can obtain the spatiotemporal temperature maps as well as the mean and median temperatures of the combustion event from each different film type. This data is displayed in Fig. 5.

Temperature mapping and plots over time show that incorporating thermite material reduces flame speed, but it also increases the temperature of the flame front and the overall combustion event. While Al/PVDF films and those incorporating low particle loadings of Bi_2O_3 and Fe_2O_3 burn at temperatures between 1400 and 1600 K, those containing CuO burn hottest with temperatures reaching near 2500 K at the higher mass loading [12]. This diagnostic technique for simultaneous acquisition of flame speed and flame temperatures allows one to get a rough idea of the relative energy release rates of each energetic composite. The ratios of the energy release rates, Q , can be calculated using the measured mass density, ρ , of each film, their respective flame speeds, v_f , and their mean flame temperatures, T_f . Assuming there is a negligible difference between the cross-sectional area of each film type, the resulting ratio is defined by Eq. (7). The specific heat of each system, \bar{c}_p , is calculated by considering respective mass fractions and the temperature averaged thermochemical values of each component found in literature and the NIST Webbook [27,28]. The specific heat of PVDF has been listed by vendors, such as Holscot and Solvay Specialty Polymers, to be roughly 1.4 (J/(g·K)). The calculated heat release ratio of metal oxide integrated films compared to stoichiometric Al/PVDF are displayed in Table 2.

$$\frac{Q_1}{Q_2} = \frac{\rho_1 v_{f1} \bar{c}_{p1} (T_{f1} - T_0)}{\rho_2 v_{f2} \bar{c}_{p2} (T_{f2} - T_0)} \quad (7)$$

These results show that there is an overall trend of a reduction to the energy release rates with the inclusion of metal oxides. The largest ratio of energy release rate occurs for the low loading of the Al/ Bi_2O_3 /PVDF at a 4% increase. However, it is difficult to solidify this as such given the degree of propagated error stemming from temperature, density, and flame speed measurements. For Al/MO/PVDF films to consistently achieve higher energy release ratios, simply adding more thermite is not enough. One must be able to control the level of film porosity in order to predictively increase film density while achieving a similar flame speed and temperature. Thus, adding stoichiometric amounts of Al/MO to Al/PVDF for mass loadings up to 67 wt% in this manner does not change the energy release rates of the energetic composite in any significant capacity.

One may also discern the degree of gas generation which manifests itself in Fig. 5 as the inability of the CCP to precisely assign a temperature value to the brown pixels. CCP is meant for temperature measurements of hot solid grey bodies, with brown pixels representing locations where large amounts of hot gas result in high temperature uncertainties, excluding them from the average temperature calculations [22]. The degree of gas generation qualitatively increases with increasing metal oxide content as well as the ability of the metal oxide to release oxygen and/or produce transient gas product species. This behavior is highlighted primarily in Fig. 5f where the film with the highest content of CuO displays a unique burning behavior resulting in a 1000 K wide mean temperature distribution as well as two distinct modes of median temperature values. The two median temperature modes are a quantitative manifestation of the previously described behavior illustrated in Fig. 4. Vigorous gas generation results in material from the flame front being shed so quickly that it continues to burn independently of the main, hotter burning reaction front. As such,

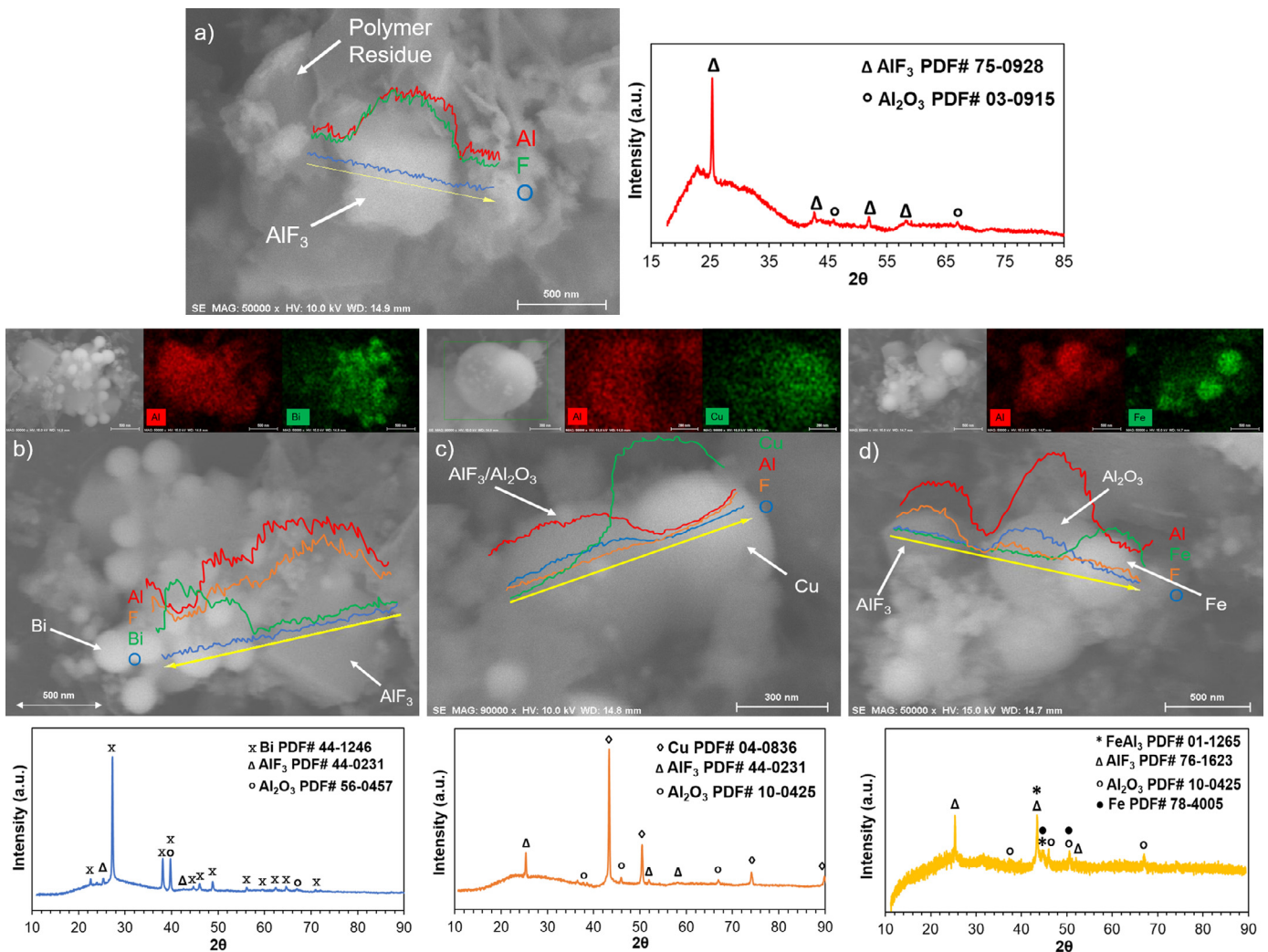


Fig. 3. Combustion products analysis (SEM, EDS, XRD) of a) Al/PVDF, b) Al/Bi₂O₃/PVDF, c) Al/CuO/PVDF, and d) Al/Fe₂O₃/PVDF films ignited in an argon atmosphere.

Table 2
Film energy release comparison compared to Al/PVDF.

| Sample (wt.%) | T _F (K) | \bar{c}_p (J/(g·K)) | Energy Release Ratio |
|---|--------------------|-----------------------|----------------------|
| Al(25)/PVDF(75) | 1370±30 | 1.33 | 1.00 |
| Al(26.5)/Fe ₂ O ₃ (23.5)/PVDF(50) | 1500±100 | 1.21 | 0.87±0.16 |
| Al(23.9)/CuO(26.1)/PVDF(50) | 1750±150 | 1.15 | 0.99±0.21 |
| Al(23.2)/CuO(43.5)/PVDF(33.3) | 2200±200 | 1.03 | 0.91±0.26 |
| Al(20.8)/Bi ₂ O ₃ (29.2)/PVDF(50) | 1470±50 | 1.01 | 1.04±0.16 |
| Al(18.1)/Bi ₂ O ₃ (48.6)/PVDF(33.3) | 1550±75 | 0.80 | 0.61±0.10 |

calculation results in Table 2 for the high loading of Al/CuO/PVDF only consider the upper band of median temperature values since they correlate to the temperature of the main flame front.

3.3. T-Jump/TOFMS analysis of Al/MO/PVDF films

Ignition properties and transient gas phase speciation of Al/MO/PVDF films were characterized using T-Jump/TOFMS at rapid heating rates in 1 atm argon and vacuum ($\sim 10^{-6}$ Torr). It must be noted that while T-Jump ignition analysis maybe performed in various gas environments, TOFMS may only be performed in vacuum. The ignition temperature of both the thermite powder and the thermite within the polymer were measured in each atmosphere and plotted against one another to probe the role of the thermite within the composites with respect to film ignition. Quantitative

results are shown in Fig. 6 with film and thermite powder ignition behavior depicted in Figure S12 and Figure S13.

The ignition results in argon show that the inclusion of the metal oxide in Al/PVDF has a negligible effect on the ignition temperature when compared to Al/PVDF ignition which occurs at ~ 620 °C. However, in vacuum, the inclusion of metal oxide particles has a clear impact on film ignition behavior where the ignition temperature is generally higher and closely correlated to the ignition of the powder thermite (Fig. 6). Additionally, it does not appear that Al/PVDF ignites at all in vacuum (Figure S12).

As previously discussed, the interaction of HF gas with the oxide layer of aluminum nanoparticles has shown to be a key facilitator in the fluorination of aluminum [8]. In a vacuum environment, the diffusivity of nascent gas species is at least 8 orders of magnitude greater than at atmospheric conditions. Nascent gas is

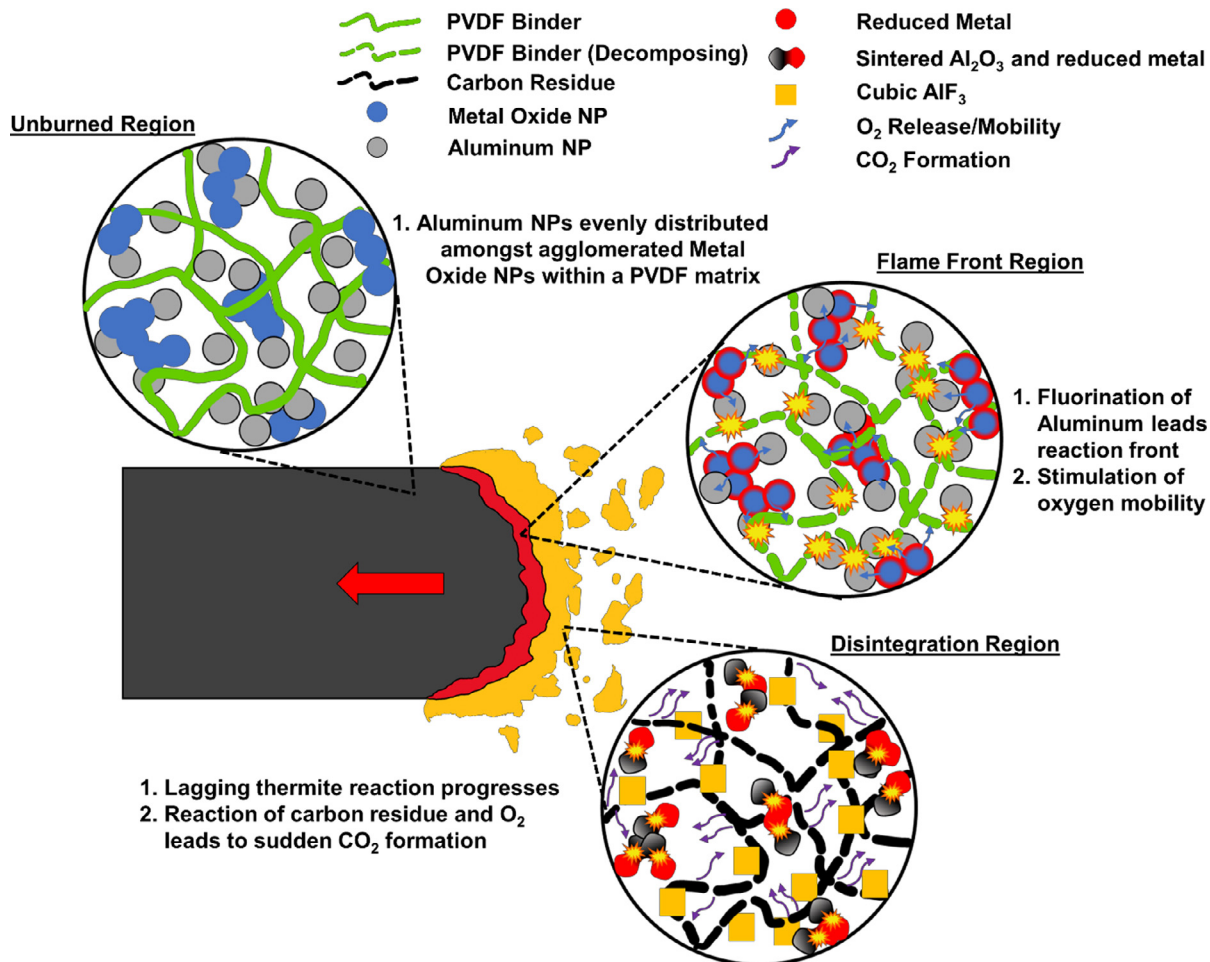


Fig. 4. Illustration of the proposed mechanism for the observed burning behavior of Al/MO/PVDF films.

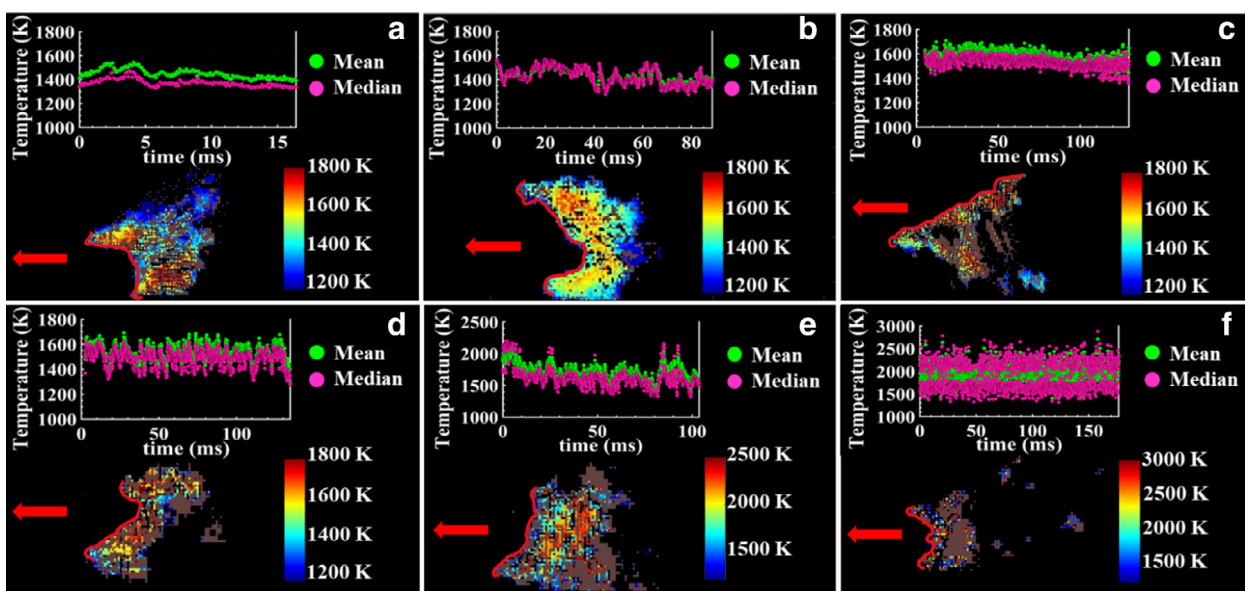


Fig. 5. Snap shots of spaciotemporal temperature measurements made by color camera pyrometry on a) Al/PVDF, b) Al/Bi₂O₃/PVDF (50 wt% particles), c) Al/Bi₂O₃/PVDF (67 wt% particles), d) Al/Fe₂O₃/PVDF (50 wt% particles), e) Al/CuO/PVDF (50 wt% particles), and f) Al/CuO/PVDF (67 wt% particles) films burning from right to left.

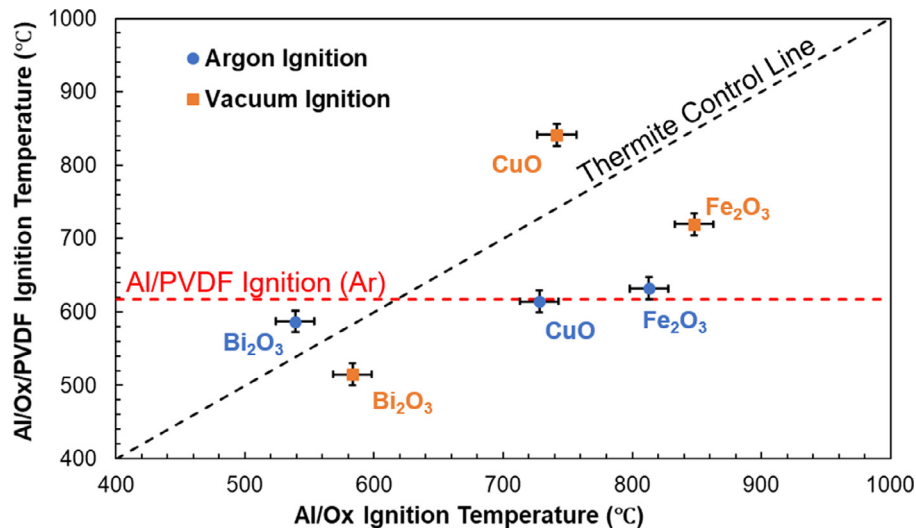


Fig. 6. Ignition temperature of metal oxide specified powdered thermite relative to the ignition temperature of thermite integrated into Al/PVDF composites in argon and vacuum.

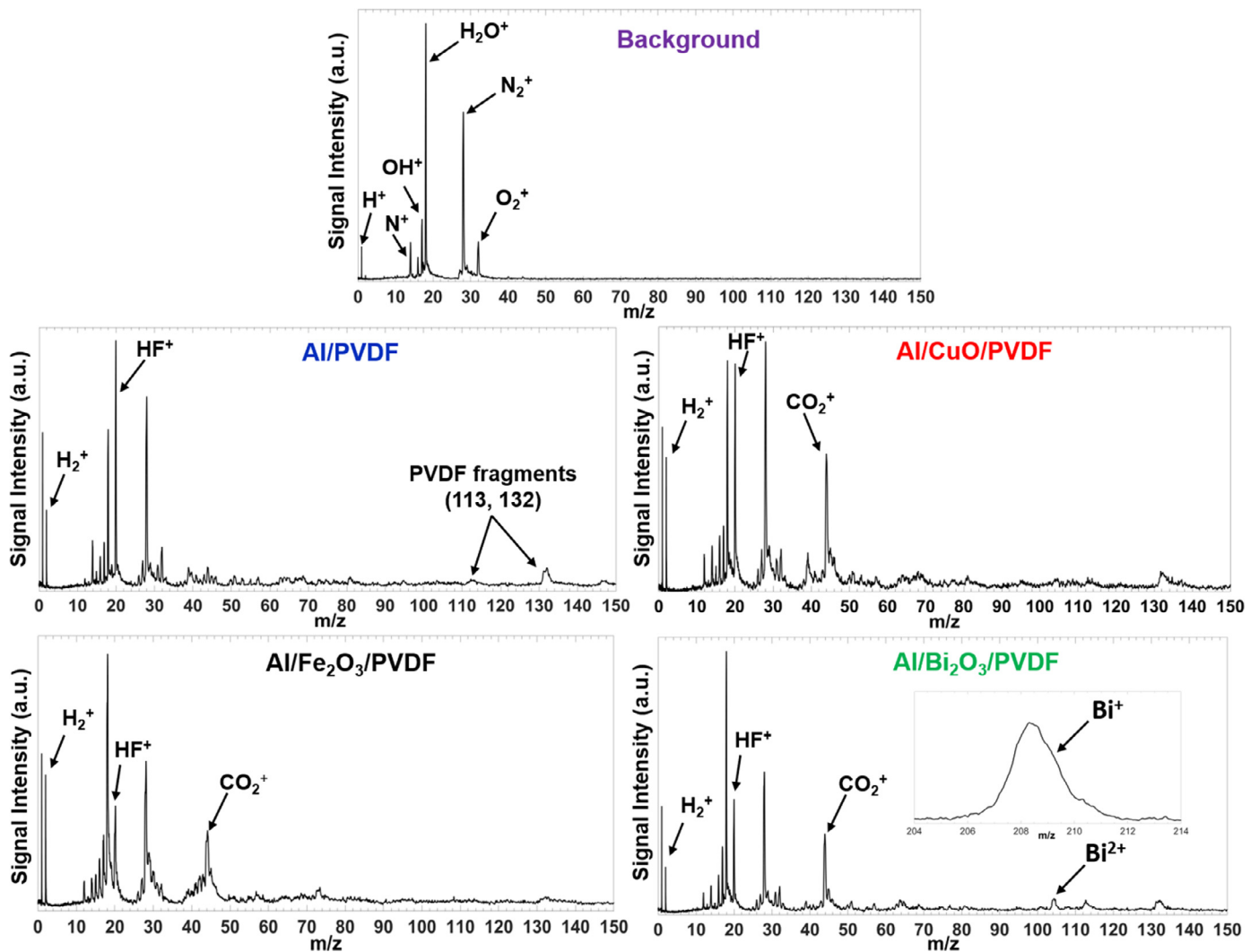


Fig. 7. T-Jump/TOFMS Mass spectra of Al/MO/PVDF composites averaged over 10 ms.

effectively in the ballistic regime, making a swift exit away from the reaction zone around the wire before being able to effectively interact with aluminum. Supplemental temporal HF speciation data, provided by TOFMS in Figure S14, shows that HF gas is released as early as 460 °C, before ignition for all composites. The lack of ignition in vacuum reinforces that the Al/PVDF reaction is mediated by a gas phase interaction. The pre-ignition reaction is thus enhanced as the diffusivity of HF gas decreases in pressurized environments, resulting in more violent, binder constrained ignition events such as those in Figure S12. However, the films that do ignite in vacuum do so with the aid of the Al/MO reaction. It is in this way that ignition in vacuum is thermite controlled.

Figure 7 illustrates the full 10 ms averaged mass spectrum from T-Jump/TOFMS analysis of all energetic compositions for which many other gas phase species, both transient and omnipresent, are detected.

In addition to background air components, rapid heating of Al/PVDF reveals the decomposition species of PVDF in the form of HF gas ($m/z=20$), molecular hydrogen ($m/z=2$), and other high mass gas species described in a previous paper [8]. The mass spectra of the metal oxide containing films also show the clear emergence of carbon dioxide ($m/z=44$) and even vaporized bismuth ($m/z=209$) in the case of Bi_2O_3 . Upon decomposition, PVDF decomposes to form carbon species which could provide a fuel source other than aluminum which can react with oxygen nascent from the metal oxide [8,9,18]. The possible interaction between the metal oxide and PVDF was further considered in which MO/PVDF composites were subject to T-Jump/TOFMS with the results displayed in Figure S15. The mass spectra from TOFMS once again displays the emergence of carbon dioxide, indicating the consumption of oxygen by the newly available carbon-based fuel.

By comparison, T-Jump/TOFMS of bare CuO results in a sudden release of oxygen which dwarfs the signal intensity of all other species present (Figure S15). Instead of a large oxygen release signal, CuO/PVDF displays the largest CO_2 signal out of all the other compositions studied. Combined with SEM evidence of Al_2O_3 formation, this suggests that the metal oxide is reacting with both the aluminum fuel and carbon species nascent from PVDF decomposition. The availability of these nascent carbon species in pressurized environments is also suggested by the increased flame speed and vigor by which Al/PVDF films burn in air (Figure S3b) [3]. Films formulated in this study are thus inherently fuel rich and contributes to combustion performance deterioration as more metal oxide content reacts with carbon species instead of the provided aluminum.

Rectifying the stoichiometric imbalance internally without the assistance of oxygen from air while maintaining and improving mechanical integrity will prove to be a challenging endeavor. Further in-depth studies with respect to the interaction of the MO/PVDF content will need to be undertaken to better understand how they may affect the overall combustion performance with a metal fuel. The solution for wider variations in flame speed and energy release tunability maybe accomplished through architectural structure-function methods and/or modifying the printing process to include a wider variety of relevant film friendly constituents.

4. Conclusions

This study investigated the formulation and combustion performance of ink extrusion 3D printed energetic films incorporating high mass loadings of aluminum and relevant metal oxide nanoparticles within a PVDF binder. It was found that each of the resulting two component films were homogeneously mixed with a high degree of geometric reproducibility between films with differing particle type and loading. However, as more thermite content is included, the mechanical integrity of the films is reduced and

dependent on the physical characteristics of the added metal oxide nano-powder.

The ignition temperature in an argon atmosphere was shown to be controlled by the Al/PVDF reaction whereas the ignition temperature in vacuum is controlled by the Al/MO reaction. These results reinforce the necessity for a HF mediated gas phase reaction mechanism of Al/PVDF. Both ignition in vacuum and intrinsic energy release rates appear to be dependent on the type of metal oxide utilized. However, there does not appear to be much variation among the metal oxides with respect to self-propagating flame speeds in argon at atmospheric pressure. Overall, increased thermite mass content in solvent based fabrication leads to increased porosity, decreased flame speeds, increased flame temperature, and diminished energy release rates.

Integrated metal oxides appear to not only react with aluminum but also carbon species formed from PVDF decomposition, generating CO_2 and deviating from the predetermined mutually exclusive stoichiometric balance in the system. Differences in Al/PVDF and Al/MO kinetics, and film disintegration from increased gas generation appear to be adverse factors for film combustion performance.

Energetically active additives of differing forms, other than metal oxides, may be supplemented by niche non-energetic constituents for future formulations which seek to enhance burning rates in a predetermined manner. Knowledge of the thermal diffusivity would be of great importance for future studies of the kinetics of such systems. Tuning content which facilitates kinetics and the mobility of chemically generated heat, and systematically varying film architecture for the promotion of efficient thermal transport are necessary to the promotion of both flame velocity and energy release rates.

Acknowledgments

The authors gratefully acknowledge support from the AFOSR. We acknowledge the support of the Maryland Nanocenter and its NispLab. The NispLab is supported in part by the NSF as a MRSEC Shared Experimental Facility.

Supplementary materials

Supplementary material associated with this article can be found, in the online version, at doi:[10.1016/j.combustflame.2019.08.023](https://doi.org/10.1016/j.combustflame.2019.08.023).

References

- [1] J. DeLisio, Understanding the relationships between architecture, chemistry, and energy release of energetic nanocomposites, Department of Chemical and Biomolecular Engineering and Department of Chemistry and Biochemistry, University of Maryland, College Park, College Park, Maryland, 2017, p. 194.
- [2] G. Young, H.Y. Wang, M.R. Zachariah, Application of nano-aluminum/nitrocellulose mesoparticles in composite solid rocket propellants, *Propellants Explos. Pyrotech.* 40 (2015) 413–418.
- [3] C. Huang, G.Q. Jian, J.B. DeLisio, H.Y. Wang, M.R. Zachariah, Electro spray deposition of energetic polymer nanocomposites with high mass particle loadings: a prelude to 3D printing of rocket motors, *Adv. Eng. Mater.* 17 (2015) 95–101.
- [4] R.A. Chandru, N. Balasubramanian, C. Oommen, B.N. Raghunandan, Additive manufacturing of solid rocket propellant grains, *J. Propul. Power* 34 (2018) 1090–1093.
- [5] K.A. Meeks, B.R. Clark, J.E. Cano, C.A. Applett, M.L. Pantoya, Effects of rheological properties on reactivity of energetic thin films, *Combust. Flame* 162 (2015) 3288–3293.
- [6] F.D. Ruz-Nuglo, L.J. Groven, 3-D Printing and development of fluoropolymer based reactive inks, *Adv. Eng. Mater.* 20 (2018) 8.
- [7] X.L. Hu, J.B. DeLisio, X.Y. Li, W.B. Zhou, M.R. Zachariah, Direct deposit of highly reactive $\text{Bi}(\text{IO}_3)_3$ -polyvinylidene fluoride biocidal energetic composite and its reactive properties, *Adv. Eng. Mater.* 19 (2017) 9.
- [8] J.B. DeLisio, X.L. Hu, T. Wu, G.C. Egan, G. Young, M.R. Zachariah, Probing the reaction mechanism of aluminum/poly(vinylidene fluoride) composites, *J. Phys. Chem. B* 120 (2016) 5534–5542.

- [9] R. Padhye, A.J.A. Aquino, D. Tunega, M.L. Pantoya, Fluorination of an alumina surface: modeling aluminum-fluorine reaction mechanisms, *ACS Appl. Mater. Interfaces* 9 (2017) 24290–24297.
- [10] D.T. Osborne, M.L. Pantoya, Effect of al particle size on the thermal degradation of al/teflon mixtures, *Combust. Sci. Technol.* 179 (2007) 1467–1480.
- [11] X.Y. Li, P. Guerieri, W.B. Zhou, C. Huang, M.R. Zachariah, Direct deposit laminate nanocomposites with enhanced propellant properties, *ACS Appl. Mater. Interfaces* 7 (2015) 9103–9109.
- [12] K. Sullivan, M.R. Zachariah, Simultaneous pressure and optical measurements of nanoaluminum thermites: investigating the reaction mechanism, *J. Propul. Power* 26 (2010) 467–472.
- [13] X.Z. Wang, W.B. Zhou, J.B. DeLisio, G.C. Egan, M.R. Zachariah, Doped delta-bismuth oxides to investigate oxygen ion transport as a metric for condensed phase thermite ignition, *PCCP* 19 (2017) 12749–12758.
- [14] G.Q. Jian, S. Chowdhury, K. Sullivan, M.R. Zachariah, Nanothermite reactions: is gas phase oxygen generation from the oxygen carrier an essential prerequisite to ignition? *Combust. Flame* 160 (2013) 432–437.
- [15] N.W. Piekielek, L. Zhou, K.T. Sullivan, S. Chowdhury, G.C. Egan, M.R. Zachariah, INITIATION and reaction in al/bi₂O₃ NANOTHERMITES: evidence for the predominance of condensed phase chemistry, *Combust. Sci. Technol.* 186 (2014) 1209–1224.
- [16] S.C. Ligon, R. Liska, J. Stampfl, M. Gurr, R. Mulhaupt, Polymers for 3D printing and customized additive manufacturing, *Chem. Rev.* 117 (2017) 10212–10290.
- [17] J. McCollum, A.M. Morey, S.T. Iacono, Morphological and combustion study of interface effects in aluminum-poly(vinylidene fluoride) composites, *Mater. Des.* 134 (2017) 64–70.
- [18] T.J. Fleck, M.A. K., I.E. Gunduz, S.F. Son, G.T.-C. Chiu, J.F. Rhoads, Additive manufacturing of multifunctional reactive materials, *Addit. Manuf.* 17 (2017) 176–182.
- [19] A.K. Murray, W.A. Novotny, T.J. Fleck, I.E. Gunduz, S.F. Son, G.T.-C. Chiu, J.F. Rhoads, Selectively-deposited energetic materials: a feasibility study of the piezoelectric inkjet printing of nanothermites, *Addit. Manuf.* 22 (2018) 69–74.
- [20] K.T. Sullivan, C. Zhu, E.B. Duoss, A.E. Gash, D.B. Kolesky, J.D. Kuntz, J.A. Lewis, C.M. Spadaccini, Controlling material reactivity using architecture, *Adv. Mater.* (2016) 1934–1939.
- [21] M. Singh, A.P. Haring, Y. Tong, E. Cesewski, E. Ball, R. Jasper, E.M. Davis, B.N. Johnson, Additive manufacturing of mechanically isotropic thin films and membranes via microextrusion 3D printing of polymer solutions, *ACS Appl. Mater. Interfaces* (2019) In press, doi:10.1021/acsami.1028b22164.
- [22] R.J. Jacob, D.J. Kline, M.R. Zachariah, High speed 2-dimensional temperature measurements of nanothermite composites: probing thermal vs. Gas generation effects, *J. Appl. Phys.* 123 (2018) 115902.
- [23] M.C. Rehwoldt, Y. Yang, H.Y. Wang, S. Holdren, M.R. Zachariah, Ignition of nanoscale titanium/potassium perchlorate pyrotechnic powder: reaction mechanism study, *J. Phys. Chem. C* 122 (2018) 10792–10800.
- [24] L. Zhou, N. Piekielek, S. Chowdhury, M.R. Zachariah, T-Jump/time-of-flight mass spectrometry for time-resolved analysis of energetic materials, *Rapid Commun. Mass Spectrom.* 23 (2009) 194–202.
- [25] A. van der Heijden, Developments and challenges in the manufacturing, characterization and scale-up of energetic nanomaterials - A review, *Chem. Eng. J.* 350 (2018) 939–948.
- [26] G.Q. Jian, L. Zhou, N.W. Piekielek, M.R. Zachariah, Low effective activation energies for oxygen release from metal oxides: evidence for mass-transfer limits at high heating rates, *ChemPhysChem* 15 (2014) 1666–1672.
- [27] L.A. Irtyugo, N.V. Belousova, V.M. Denisov, S.D. Kirik, L.G. Chumilina, High-Temperature heat capacity of bismuth oxide and bismuth-zinc double oxide with the sillenite structure, *J. Siberian Federal Univ.* 2 (2012) 125–130.
- [28] Y. Berezovskaya, S. Budurov, T. Spasov, Specific heats of fcc solid solutions of the Bi₂O₃-Y₂O₃ system, *Cryst. Res. Technol.* 22 (1987) 1415–1419.